Supplementary Information

Antibody-Functionalized Fluid-Permeable Surfaces for Rolling Cell Capture at High Flow Rates

Sukant Mittal, Ian Y. Wong, William M. Deen and Mehmet Toner

Device Fabrication

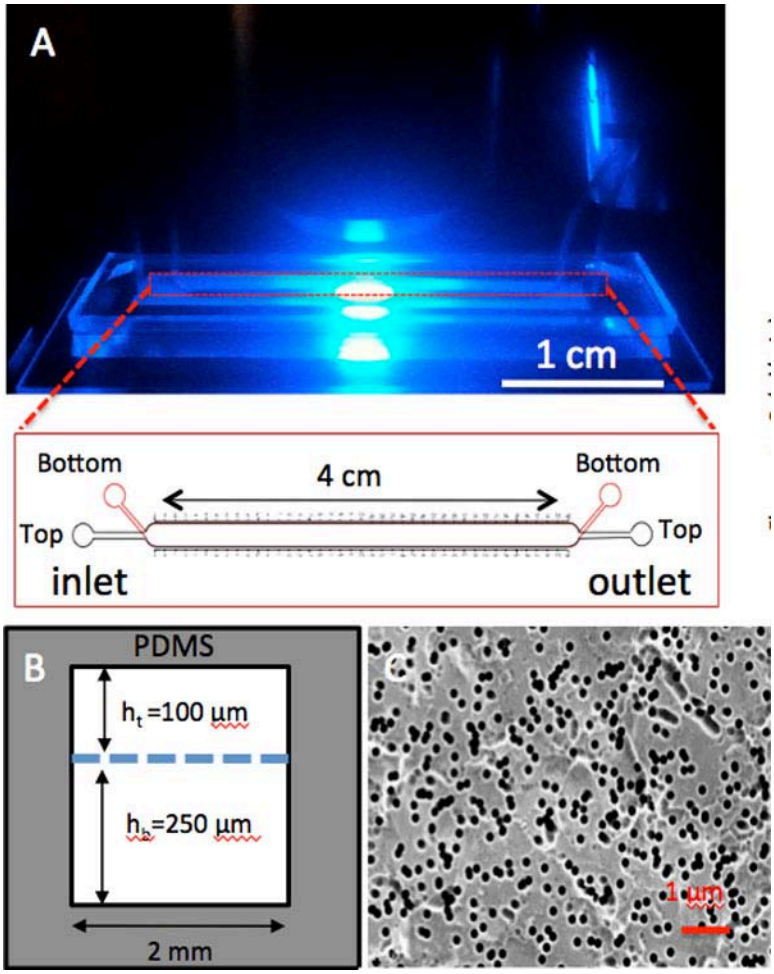

Fig. S1. Microfluidic devices consisted of a polycarbonate membrane sandwiched between two PDMS channels, following the technique described by Chueh et al. *Anal Chem*, 79, 3504-3508, (2007).[51] (a) Channels were 4 cm long with independent inlets and outlets for top and bottom. (b) The top channel was 100 µm high, while the bottom channel was 250 µm high. The bottom channel was taller than the top channel to allow fluid permeation through the membrane. Both channels were 2 mm wide. (c) Polycarbonate membranes (GE Whatman, Piscataway, NJ) were 10 µm thick, with an average pore size of ~200 nm and 10% porosity.

Supplementary Information

Antibody-Functionalized Fluid-Permeable Surfaces for Rolling Cell Capture at High Flow Rates

Sukant Mittal, Ian Y. Wong, William M. Deen and Mehmet Toner

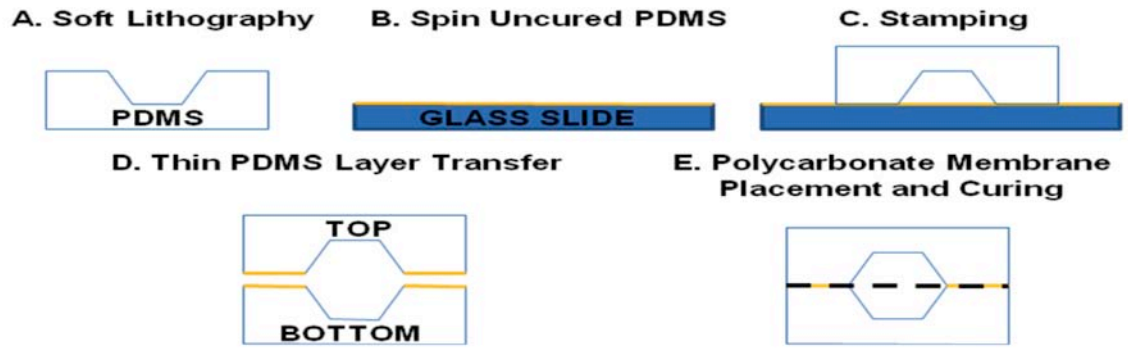

Fig. S2. (a) Negative photoresist (SU-8, MicroChem, Newton, MA) was photolithographically patterned on silicon wafers to create masters. The masters were then used as molds, on which polydimethylsiloxane (PDMS) prepolymer (Sylgard 184, Dow Corning, Midland, MI) mixed with its crosslinker at 10∶1 (Sylgard, 184, Dow Corning) weight ratio was poured, degassed, and allowed to cure in a conventional oven at 65 ºC for 24 h before removal from the molds. (b) Next, a thin layer of uncured PDMS diluted in toluene (50% v/v) (Sigma Aldrich, St. Louis, MO) was spun 1800 rpm for 1 min onto a glass slide using a high-speed spinner. (c) The thin layer of PDMS was transferred onto the channel surfaces by gently stamping the PDMS channel onto the uncured PDMS. (d) The polycarbonate membrane(GE Whatman) was gently placed over the bottom channel first and then the top channel was carefully aligned over it. (e) The device constructs was allowed to sit at room temperature overnight to cure at 70°C.

The polycarbonate membranes were then covalently functionalized with Anti-EpCAM (R&D Systems, Minneapolis, MN) or IgG (30 μg/mL) (R&D Systems) using a method previously described by Suye et al., Biotechnol. Appl. Biochem, 27, 245-248 (1998). Briefly, after glutaraldehyde (Electron Microscopy Services, Hatfield, PA) incubation of the microfluidic channel, the device was thoroughly washed with phosphate buffer saline (Invitrogen, Carlsbad, CA) and incubated with 20 μg/mL of Avidin (Thermo Scientific, Rockford, IL). The device was then washed with buffer and the top channel of the device was then incubated with biotinylated anti-EpCAM or IgG for 2 hours. The antibody was washed with phosphate buffer and the device was incubated with 5% Pluronic F108 (Fisher Scientific, Pittsburg, PA) in 2 % BSA (Sigma Aldrich) in order to reduce non-specific binding of cells.

Supplementary Information

Antibody-Functionalized Fluid-Permeable Surfaces for Rolling Cell Capture at High Flow Rates

Sukant Mittal, Ian Y. Wong, William M. Deen and Mehmet Toner

Sample Preparation

Leukocytes ("buffy coat") were isolated from whole blood using deterministic lateral displacement (32) and resuspended to a concentration of 500,000/mL. These cells were fluorescently labeled (CellTracker calcein green, Invitrogen) following the manufacturer protocol. PC3 human prostate cancer cells (ATCC) were cultured at 37ºC and 5% CO2 in F-12K growth media containing 1.5 mM L-glutamine supplemented with 10% FBS and 1% Penicillin/Streptomycin, with media changes every 2–3 days. These cells were labeled with a different fluorescent dye (Cell Tracker Orange, Invitrogen) and spiked into the sample at a ratio of 1:250 (2000/mL). The PC3 spike count was verified immediately before addition to the buffy coat population as well as before loading the sample into the device. These readings were consistent to within 5%. After capture, cells were nuclear stained with DAPI (Invitrogen) following manufacturer protocol.

Fluid flux split control

Since the optimal working of the device depends on the fluid flux through the top channel and the membrane, it is important to reproducibly achieve the same fluid field conditions in order to compare different devices. In Figure 1d, the flow rates through top and bottom channels scale linearly with applied pressure difference. Moreover, the ratio of flow rates in the top and bottom channels is constant, governed by the high resistance outputs. The calibration and model are further described below.

Supplementary Information

Antibody-Functionalized Fluid-Permeable Surfaces for Rolling Cell Capture at High Flow Rates

Sukant Mittal, Ian Y. Wong, William M. Deen and Mehmet Toner

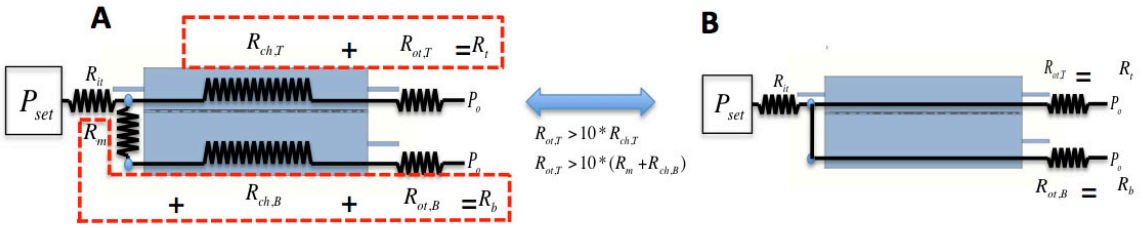

Fig. S2a, b shows the lumped resister model for device operation. It reduces the percentage permeation flux variations and quantify the performance of the device reproducibly with the addition of large resistive tubings (r_t=50 μm) at the top and bottom channels helped "short" out any inherent variations in the commercially available membranes and insured constant permeation flux along the length of the membrane. The model was able to accurately predict the fluid split between the top and the bottom channels as a function of the sample input pressure when the tubing resistances were approximately ten times the fluidic resistance of the membrane and the channels in a sample with dilute suspension of particles ($\phi_o < 0.1$). The ratio of the resistances on the top and bottom tubings determine the fluid split, whereas the actual resistances of the tubings determine the sample flow rate through the top and bottom outlets of the channels. The different component fluidic resistances of the device are shown in Table S.1. The channel resistances were calculated using Eqn. S.1

$$R_{ch} = \frac{12\mu L_{ch}}{wh^3} \quad \text{(S.1)}$$

The tubing resistances were calculated using Eqn. S.2

$$R_{tubing} = \frac{8\mu L_t}{\pi {r_t}^4} \quad \text{(S.2)}$$

The membrane resistances were calculated using Eqn S.3

$$R_m = \frac{8\mu L_p}{\pi {r_p}^4} . \frac{1}{n} \quad \text{(S.3)}$$

Based on the above resistances, the theoretical flow rates in the top channel and membrane are given by

$$Q_t = \frac{R_b P}{(R_{in}(R_b + R_t) + R_b R_t)} \quad \text{(S.4)}$$

$$Q_b = \frac{R_t P}{(R_{in}(R_b + R_t) + R_b R_t)} \quad \text{(S.5)}$$

Supplementary Information

Antibody-Functionalized Fluid-Permeable Surfaces for Rolling Cell Capture at High Flow Rates
Sukant Mittal, Ian Y. Wong, William M. Deen and Mehmet Toner

Where,

$$R_t = R_{ch,T} + R_{ot,T} \quad \text{(S.6)}$$

$$R_b = R_m + R_{ch,B} + R_{ot,B} \quad \text{(S.7)}$$

If,

$$R_{ot,T} > 10R_{ch,T}, R_{ot,B} > 10(R_m + R_{ch,B}) \; R_{ot,T} > 10R_{ch,T}, R_{ot,B} > 10(R_{ch,B} + R_{ot,B}) \quad \text{(S.8)}$$

Then,

$$R_t = R_{ot,T} \quad \text{(S.9)}$$

$$R_b = R_{ot,B} \quad \text{(S.10)}$$

$$A = \frac{Q_b}{Q_t + Q_b} = \frac{R_t}{R_t + R_b} \quad \text{(S.11)}$$

The resistance values in Table S.1 show that the output tubings have resistance much greater (~10 times) than the fluidic resistance of the channel or the membrane. Under this condition, the resistance model can be simplified from Fig. S2a to Fig. S2b. The effect of the simplified model is to maintain a constant pressure difference along the length of the membrane and hence a constant uniform velocity of fluid flux at the wall. Additionally, the simplified model allows prediction of the fluid split and flow rates based on the lengths and therefore the resistances of the outlet tubings. Eqn. S.6-S.11, define sample fluid flow rate through the top channel and the membrane depends on the absolute values of the top and bottom output tubing resistances, but the split depends on the ratios of the two. In the event when the outlet tubings are short in length, the flux through the top and the bottom channels varies greatly. A mean standard deviation of 0.42 ml/hr permeation flux through the membranes was measured due to porosity differences in the polycarbonate membranes.

	Inlet tubing R_{it} (Length= 50 cm)	Top Channel $R_{ch,T}$	Top Outlet tubing $R_{ot,T}$ (Length = 266 cm)	Bottom Channel $R_{ch,B}$	Bottom outlet tubing $R_{ot,B}$ (Length = 114 cm)	Membrane R_m (Average porosity ~ 10%, r_p = 0.1 μm)

Supplementary Information

Antibody-Functionalized Fluid-Permeable Surfaces for Rolling Cell Capture at High Flow Rates
Sukant Mittal, Ian Y. Wong, William M. Deen and Mehmet Toner

Fluidic Resistance	4.9×10^{12}	1.24×10^{11}	2.6×10^{13}	1.5×10^{10}	1.1×10^{13}	10^{12}

Table S.1 Component resistances of the device. The tubing resistances are kept at a much higher resistance that the channel and the membrane resistances.

Fluid Streamline and Particle Trajectory Calculations

Equations [1] and [2] in the text for the fluid streamlines and particle trajectories are derived here. The coordinates *x,y*; pressure *p*, velocity u_x and ratio of permeation flux to total flux *A* were nondimensionalized:

$$X=\frac{x}{h}, Y=\frac{y}{h}, <P>=\frac{<p>-p_o}{p_o}, <U_x>=\frac{<u_x>}{<u_o>}, A=\frac{v_w}{<u_o>}$$

According to the lubrication approximation,

$$\frac{\partial^2 u_x}{\partial Y^2}=\frac{h}{\mu}\frac{dP}{dX}, \qquad \text{BC's: } u_X(X,0)=u_X(X,1)=0 \tag{S.12}$$

The axial velocity profile in a microfluidic channel with solid walls is:

$$u_X(X,Y)=6<u_X>(Y-Y^2) \tag{S.13}$$

The fluid mass balance across an elemental section in a microfluidic device with a porous bottom surface is given by relating the average fluid velocity along the length of the channel to the fluid permeating through the membrane,

$$\frac{d<u_X>}{dX}=-\frac{v_w}{h} \tag{S.14}$$

Integrating along the length of the channel,

$$<u_X>=u_o(1-v_wX) \tag{S.15}$$

Therefore,

$$u_X(X,Y)=6u_o(1-v_wX)(Y-Y^2) \tag{S.16}$$

In its non-dimensional form,

$$U_X(X,Y)=6(1-AX)(Y-Y^2) \tag{S.17}$$

Supplementary Information

Antibody-Functionalized Fluid-Permeable Surfaces for Rolling Cell Capture at High Flow Rates
Sukant Mittal, Ian Y. Wong, William M. Deen and Mehmet Toner

The transverse fluid velocity field $u_Y(X,Y)$, can be obtained from the continuity equation

$$\frac{\partial u_X}{\partial X} + \frac{\partial u_Y}{\partial Y} = 0 \tag{S.18}$$

Integrating eqn. S.18,

$$u_Y(X,Y) = \int_Y^1 \frac{\partial u_X}{\partial X}(X,S)dS, \qquad \text{BC: } u_Y(X,1) = 0 \tag{S.19}$$

$$u_Y(X,Y) = -v_w(2Y^3 - 3Y^2) \tag{S.20}$$

In non-dimensionalized form,

$$U_Y(X,Y) = -A(2Y^3 - 3Y^2) \tag{S.21}$$

Velocity profiles for a microfluidic channel with solid walls can be obtained by setting $v_w \sim 0$.

The fluid streamlines in the rectangular channel with a porous bottom is therefore given by,

$$3Y^2 - 2Y^3 = \frac{3Y_o^2 - 2Y_o^3}{1 + AX} \tag{S.22}$$

Cell trajectories in a dilute suspension

Faxen's law provides a general relationship between force on a spherical cell (F), its velocity (u_p) and the unperturbed fluid velocity (u_o) field far from the particle center. To determine how the cell trajectory is affected by the fluid streamlines, the x- and y- component of Faxen's first law for a non-buoyant cell (density difference $\Delta\rho$=0.030 g/cm^3) were calculated:

$$F_x \sim 0 = 6\pi\mu R_c\{(u)_x - (u_p)_x + \frac{R_c^2}{6}(\nabla^2(u)_x)\} \tag{S.23}$$

$$F_y \sim \frac{4\pi R_c^3 \Delta\rho}{3} = 6\pi\mu R_c\{(u)_y - (u_p)_y + \frac{R_c^2}{6}(\nabla^2(u)_y)\} \tag{S.24}$$

where R_c = radius of the cell (5 μm). The effect of cell radius on streamline trajectory is negligible for R_c< 20μm. Therefore higher order R_c terms in eqn. S.23 and eqn. S.24 can be neglected and the Faxen's first law can be re-written as:

$$F_x \sim 0 = 6\pi\mu R_c\{(u)_x - (u_p)_x\} \tag{S.25}$$

$$F_y \sim \frac{4\pi R_c^3 \Delta\rho}{3} = 6\pi\mu R_c\{(u)_y - (u_p)_y\} \tag{S.26}$$

The particle trajectory is thus given by,

$$\frac{dy}{dx} = \frac{v_w(3Y^2 - 2Y^3) - B}{6 < u_o > (1 - v_w X)(Y - Y^2)} \tag{S.27}$$

where $B = 2R_c^2 g\Delta\rho/9\mu_0 \sim 2$ μm/s, is a constant sedimentation velocity for a particle of radius R_c = 5 μm and density difference $\Delta\rho \sim 0.030$ g/cm^3 (with respect to the solution). The cell trajectory in the microfluidic channel can be obtained by setting $v_w \sim 0$ in eqn S.27.

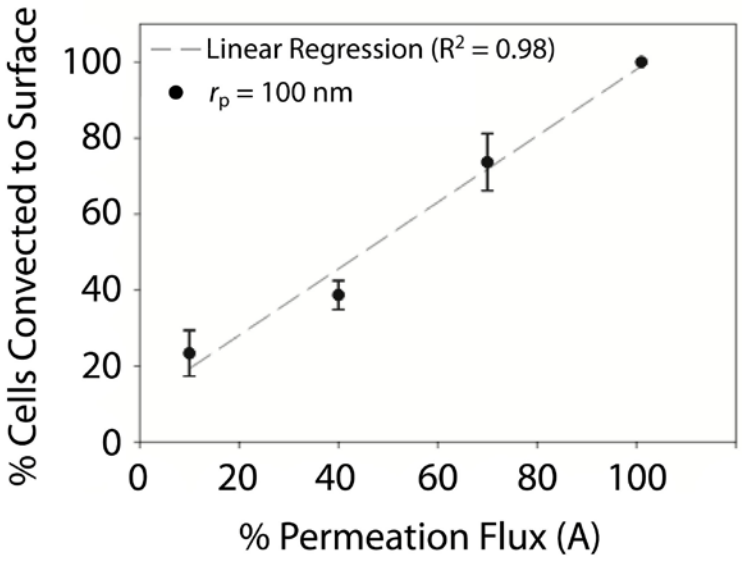

Fig. S3. Percentage of cells convected to a porous capture surface scales linearly with the percentage permeation flux. Each data point corresponds to measurements on 5 independent devices, with pore size r_p=100 nm.

Supplementary Information

Antibody-Functionalized Fluid-Permeable Surfaces for Rolling Cell Capture at High Flow Rates
Sukant Mittal, Ian Y. Wong, William M. Deen and Mehmet Toner

Comparison of Measured Cell Surface Velocity with Hydrodynamic Model

The hydrodynamics of a particle moving near a solid surface due to a shear field were previously treated theoretically by Goldman et al. *Chem. Eng. Sci.* 22, 653-660, (1967).[31] Based on the total flow rate through the channels, there should be a shear stress of 5 dyn/cm^2 at the entrance. Assuming a particle-surface separation of 50 nm, the initial cell surface velocity is expected to be $u_{c,0}$ = 1000 μm/s. This value is incorporated into a phenomenological equation based on equation [2]: $u_c(x) \sim u_{c,0}(1 - Ax / L)$. As shown in Fig. S4, the measured velocities are consistent with the hydrodynamic model at A = 50%. However, the measured values are significantly slower those predicted from the model and increasingly deviate at higher permeation rates. This discrepancy arises from the porosity of the surface, which is not accounted for in the Goldman model. The slowdown accounts from an additional "suction" force that causes temporary pauses in cell motion.

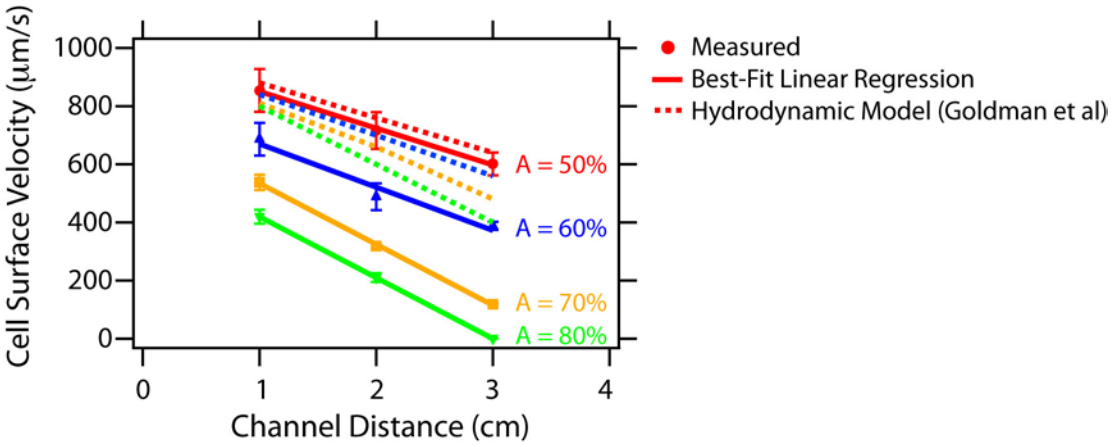

Fig S4. Comparison of measured cell surface velocity (markers), best-fit linear regression (solid lines) and hydrodynamic model of Goldman et al (dotted lines). Measured values are in agreement with model for A = 50%, but are consistently slower at larger permeation.

Supplementary Information

Antibody-Functionalized Fluid-Permeable Surfaces for Rolling Cell Capture at High Flow Rates

Sukant Mittal, Ian Y. Wong, William M. Deen and Mehmet Toner

Table S1

Permeation (A)	Distance along the channel (cm)	Shear stress (dyn/cm^2)	Hydrodynamic velocity* (μm/s)	Experimentally measured rolling velocity (μm/s)
50%	0	5	1000	-
	1	4.4	880	854 ± 74
	2	3.8	760	716 ± 63
	3	3.2	640	601 ± 39
	4	2.5	500	-
60%	0	5	1000	-
	1	4.2	840	686 ± 56
	2	3.5	700	489 ± 46
	3	2.8	560	388 ± 14
	4	2	400	-
70%	0	5	1000	-
	1	4.1	810	538 ± 27
	2	3.3	660	318 ± 5
	3	2.4	480	118 ± 3
	4	1.5	300	-
80%	0	5	1000	-
	1	4	800	420 ± 24
	2	3	600	210 ± 15
	3	2	400	0
	4	1	200	0

Table S1. Comparison of cell surface velocity on a solid flat surface and a porous surface. *Hydrodynamic velocity for unencumbered particles on a flat surface using Goldman et. al. [31] at a particle separation distance of 50 nm, a representative bond length for EpCAM antigen/antibody. Measured cell velocities are the average and standard deviation of at least 30 cells per condition.

Supplementary Information

Antibody-Functionalized Fluid-Permeable Surfaces for Rolling Cell Capture at High Flow Rates

Sukant Mittal, Ian Y. Wong, William M. Deen and Mehmet Toner

Optimizing Experimental Conditions to Maximize Capture Efficiency and Selectivity

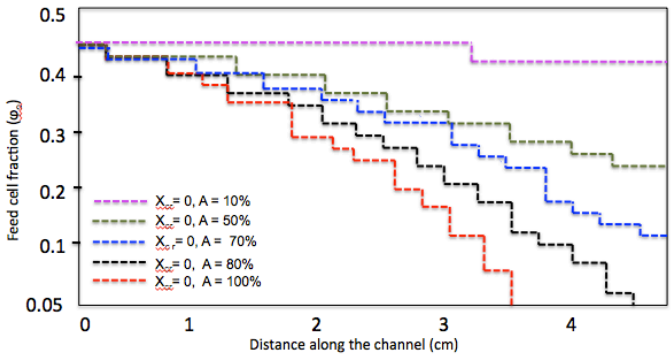

Fig S5. State diagram showing the boundaries where $x_{cr} = 0$ on the surface of the channel for different percentage permeations (A) and initial cell volume fraction (φ_o). The critical distance $x_{cr} = 0$ is reached when the volume fraction of the particles on the porous surface reaches $\varphi_w = \varphi_{max} = 0.6$